The Astrophysical Journal, 931:98 (8pp), 2022 June 1 https://doi.org/10.3847/1538-4357/ac69d3

Near-orthogonal Orientation of Small-scale Magnetic Flux Ropes Relative to the Background Interplanetary Magnetic Field

Kyung-Eun Choi[1], Dae-Young Lee[1], Katsuhide Marubashi[2], and Seunguk Lee[1]
[1] Department of Astronomy and Space Science, Chungbuk National University, Cheongju, Republic of Korea; dylee@chungbuk.ac.kr
[2] National Institute of Information and Communications Technology, Tokyo, Japan
Received 2022 January 17; revised 2022 March 28; accepted 2022 April 21; published 2022 May 27

Abstract

Small-scale magnetic flux ropes (SMFRs) have been identified at a large range of heliospheric distances from the Sun. Their features are somewhat similar to those of larger-scale flux rope structures such as magnetic clouds (MCs), while their occurrence rate is far higher. In this work, we examined the orientations of a large number of SMFRs that were identified at 1 au by fitting to the force-free model. We find that, while most of the SMFRs lie mostly close to the ecliptic plane, as previously known, their azimuthal orientations relative to the Sun–Earth line are found largely at two specific angles (slightly less than 45° and 225°). This latter feature in turn leads to a strong statistical trend in which the axis of SMFRs lies at a large tilt angle relative to (most often nearly orthogonal to) the corresponding background interplanetary magnetic field directions in the ecliptic plane. This feature is different from previous reports on SMFRs—and in stark contrast to the cases of MCs. This is an important observational constraint that should be considered for understanding SMFR generation and propagation.

Unified Astronomy Thesaurus concepts: Solar wind (1534); Interplanetary physics (827)

1. Introduction

The small-scale magnetic flux ropes (SMFRs) in the solar wind are known to have properties similar to those of the well-known magnetic clouds (MCs), but they have been observed more frequently than MCs (e.g., Yu et al. 2016; Hu et al. 2018; Choi et al. 2021) and in a large range of heliospheric distances from <0.2 au to several au from the Sun (Cartwright & Moldwin 2010; Chen & Hu 2020; Chen et al. 2020). They have been identified and modeled by a few different methods, including fitting with the force-free model (e.g., Moldwin et al. 2000; Feng et al. 2008), Grad–Shafranov reconstruction (e.g., Zheng et al. 2017), and magnetic helicity (Zhao et al. 2020a, 2020b).

Their origin remains under debate, but several suggestions exist. First, at least some of them may be a manifestation of small solar ejecta that maintain a small size while propagating (Rouillard et al. 2011). Additionally, magnetic reconnection either near or far from the Sun, particularly near the heliospheric current sheet (HCS), has been invoked as a key physics for the origin of SMFRs (Moldwin et al. 2000; Cartwright & Moldwin 2008; Drake et al. 2020; Lavraud et al. 2020; Réville et al. 2020). Another suggestion that is entirely based on interplanetary mechanisms attributes SMFRs to the product of solar wind turbulence (Greco et al. 2009; Telloni et al. 2016; Zheng & Hu 2018).

Our recent work based on suprathermal electron data (Choi et al. 2021) has shown that, for a majority of low-β SMFRs, the flux rope field lines are open with only one end connected to the Sun, and only a limited number of SMFRs have real closed field lines. In the present work, we proceed to further understand the geometrical structure of SMFRs. Specifically, we focus on determining the orientation of SMFRs for a large number of events selected by force-free model fitting. This work is motivated by our conjecture that SMFR orientation may be an important factor closely related to the origin and propagation of SMFRs. In addition, the orientation of SMFRs near the Earth is important from the viewpoint of geoeffectiveness, as they may contain a southward Bz component that triggers substorms (Feng et al. 2010; Kim et al. 2017; Park et al. 2018). If, for some reason, their orientation turns out to be statistically well-organized, this would be a crucial factor for improving space weather forecast capabilities.

The present work is distinguished from previous works in the sense that we pay attention to SMFR orientations relative to their corresponding background interplanetary magnetic field (IMF) directions, which we determine for each of the SMFRs separately. This leads us to a new statistical result different from those of previous works—and in stark contrast to those for MCs. The methods employed and statistical results are presented in Sections 2 and 3, respectively. The results in Section 3 include a comparison with those for MCs that were studied in the same way. In the last section, we point out differences from previous works and discuss a few available scenarios of SMFR origin, to assess the extent to which they may fit into the current results.

2. Methodology

In the present work, we first started from the small transient events (STs) identified by Yu et al. (2016) from the observations by the Wind, STEREO-A, and STEREO-B spacecraft at 1 au. Those events satisfy the following criteria: (i) duration between [0.5, 12] hr, (ii) magnetic field strength higher than the yearly average, specifically by a factor of 1.3, (iii) low proton beta (β_p less than 0.7 times the yearly average) or low proton temperature (T_p/T_{exp} less than 0.7, where T_{exp} is the expected proton temperature for solar wind expansion each year), and (iv) low Alfvén Mach number (M_A less than 0.7 times the yearly average) or large rotation of the magnetic field components (for more details, see Section 2.1 in Yu et al.

2016). Importantly, Yu et al. removed all the Alfvenic fluctuations from the list when the relation $\Delta V_\perp = \frac{\Delta B_\perp}{\sqrt{\mu_0 \rho}}$ is satisfied, where Δ represents the perturbation of the plasma flow and magnetic field vectors relative to background and $\perp$ means perpendicular to the background field. To quantitatively define Alfvenic fluctuations, they required either the correlations for three components of the flow velocity and magnetic field vectors to be greater than 0.5 or those for two components to be greater than 0.6 and that for the other one to be greater than 0.3.

Note that not all of the Yu et al. ST events are flux ropes. Accordingly, for the present work, we identified flux ropes from the Yu et al. ST list obtained from the Wind observations from 1995 to 2014 by applying force-free model fitting (e.g., Shimazu & Vandas 2002; Marubashi & Lepping 2007; Lepping et al. 2011; Nishimura et al. 2019). Rigorously, force-free modeling is justified for $\frac{|\nabla P|}{|J \times B|} \sim \frac{\mu_o P}{B^2} = \frac{\beta}{2} \ll 1$. To obtain a sufficiently large number of SMFR events for the statistical work designed in this paper, we selected SMFR events with the rather loose requirement that the average plasma beta based on protons be <1.

In total, we identified 261 SMFRs via force-free modeling. To obtain them, we required that a successful model fitting should satisfy the condition of least-mean squared error <0.3. The average impact parameter value for these SMFRs is 0.89, implying that the satellite passage is often rather distant from the center of these small-scale flux ropes.

Figure 1 shows two examples of force-free modeling applied to the small transient events of Yu et al. (2016). The event in column (a) is a case of successful modeling and thus is identified as an SMFR event. The magnetic field for this event exhibits the typical features of the magnetic field being enhanced in its magnitude and smoothly rotating in its direction (second to fifth and bottom three panels) and the plasma density N_p and β being reduced occurring within slow solar wind speed V_{sw} (middle panel). In contrast, the event in column (b) is a case where the force-free modeling result does not meet the error tolerance and thus is not identified as an SMFR event. Note that the magnetic field in the event in (b) exhibits less of a rotating feature and the profiles of fitted curves are rather flat during the event interval.

Figure 2 shows the yearly distribution of the 261 SMFRs along with the sunspot cycle and with distinction between two different helicities (to be discussed further later). Although it is not a focus here, we point out that the yearly distribution is not even, and it does not show an obvious solar cycle dependence except that the yearly number tends to be larger during solar cycle 24 than 23.

For our main goal of comparing the flux rope axis orientations with those of the corresponding background IMF, we determined an average IMF condition for each SMFR event. Specifically, we defined the background IMF interval as a one-day average prior to each SMFR event. Taking a one-day interval is more or less subjective, but we confirmed that the main results in this paper do not change with a different interval length (for example, 12 hrs) chosen as the background. If the chosen interval is too short, the average IMF value would be affected by short timescale fluctuations, whereas an interval that is too long might include an IMF polarity sector boundary. Therefore, we have to compromise in choosing an appropriate interval. If the preceding one-day time interval includes IMF polarity sector boundaries, we instead take a one-day interval after each SMFR event to refer to the background IMF direction.

Figure 3 shows the same SMFR event (two vertical lines) with fitted force-free model curves (red curves) as the one in Figure 1(a), but now with its background IMF interval (as indicated at the top of the top panel in (a)). Note that we defined the background IMF interval of one day after the end time of this SMFR event. For this event, the background IMF is a typical Parker spiral with away polarity with its azimuthal angle $\phi \sim 112°$ (fifth panel in (a) and blue arrow line in the schematic in (b)). Here, the azimuthal angle is defined as increasing counterclockwise in the ecliptic plane from the positive x-axis in the Geocentric Solar Ecliptic (GSE) coordinate system. More interestingly, it indicates that the azimuthal angle of the SMFR axis (black arrow line in the schematic in (b)) is 13°.8. This means that the azimuthal angle of the SMFR axis differs by −98°.2 (curved red arrow in the schematic in (b)) from that of the background IMF. In the next section, we show that such a large tilt angle in SMFRs relative to the background IMF directions is statistically common.

3. Statistical Results

Using force-free model fitting, we determined the axial orientations of each of the 261 SMFRs. Figure 4 shows the statistics of the elevation and azimuthal angles for the 261 SMFRs. The elevation angle result indicates that the majority of the SMFRs lie close to the ecliptic plane. The azimuthal angle distribution exhibits two clear peaks at slightly less than 45° and 225°, which are quite different from (and actually nearly orthogonal to) the average Parker spiral angles of the IMF, i.e., 135° and 315°.

Now, we specifically compare the azimuthal angles of the SMFRs with those of each corresponding background IMF direction. Their statistical distribution is summarized in the top three panels (a)–(c) of Figure 5. Specifically, panel (a) shows the color-coded number of events in the parameter space of the azimuthal angle of the SMFR axis versus the IMF azimuthal angle. The majority of the events are focused in four locations in panel (a) centered around ($\langle \mathrm{IMF}\phi \rangle$, SMFR axis ϕ) = (135°, 45°), (135°, 225°), (315°, 45°), and (315°, 225°). The $\langle \mathrm{IMF}\phi \rangle$ values of 135° and 315° correspond to two polarities, away and toward, respectively, and are approximately consistent with the azimuthal angles predicted by the Parker spiral IMF based on the measured solar wind speeds. Therefore, for these main groups of events, the relative difference between the two azimuthal angles ($\Delta\phi$) is approximately $\pm 90°$. This is more clearly presented in panel (b), showing the fraction of the events as binned by $\Delta\phi$. The same result is expressed in terms of the absolute value ($|\Delta\phi|$) in panel (c), where the mean value of $|\Delta\phi|$ is 90°.9 and the distribution peaks at $|\Delta\phi| \approx 85°$. In short, Figures 5(a)–(c) clearly indicate a newly found feature of the flux rope axis of the majority of the studied SMFRs, with a large tilt angle (most often nearly perpendicular) to the background IMF.

For comparison, we performed the same analysis of determination of azimuthal angles for MCs against IMF directions. For this, we used two lists of MC events, one selected by the Wind MFI team based on Lepping et al. (1990) (available at https://wind.nasa.gov/mfi/mag_cloud_S1.html) and another published in Nishimura et al. (2019), both of which were obtained by force-free model fitting to Wind observations. Here, they are referred to as the "Lepping list" and "Nishimura

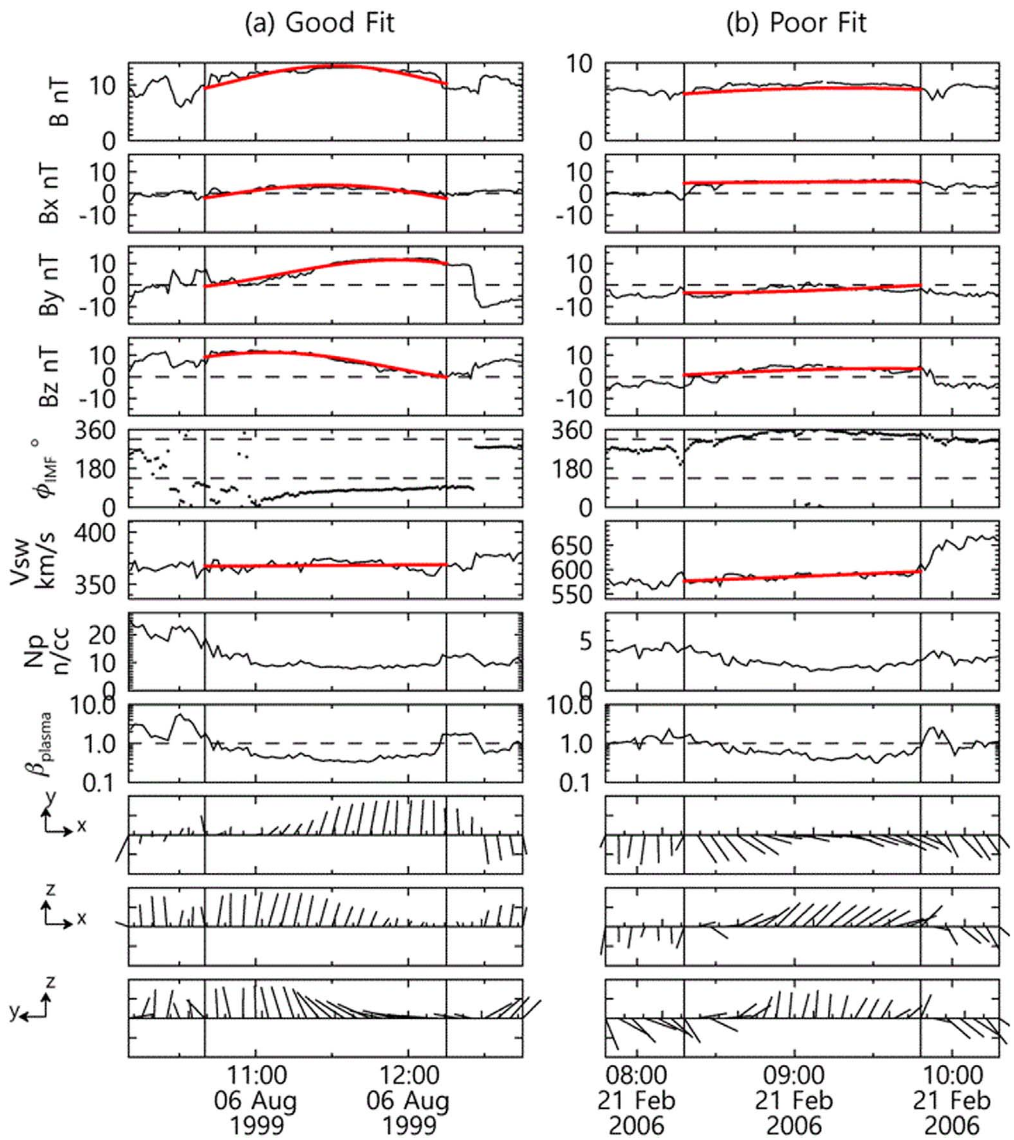

Figure 1. Two examples of force-free modeling applied to the transient events that were identified by Yu et al. (2016) using the interplanetary magnetic fields and solar wind plasma parameters measured by Wind (see text for details). The vertical lines denote the boundaries of each transient event interval, where the force-free model curves are shown as red lines and the bottom three panels in each event show the magnetic vector evolutions. (a) A case of successful force-free modeling that exhibits a smoothly rotating magnetic field feature, and thus we identify it as an SMFR event. (b) A case of less rotating magnetic field variations (rather flat profiles of fitted curves) for which the force-free modeling is not satisfactory, and thus it is not identified as an SMFR event.

list," respectively. For comparison with the present analysis for SMFRs, we use only the MC events that were obtained during the same interval as that from which our SMFRs were selected. The results of the azimuthal angle determination for the MCs are shown in the last two rows of Figure 5, which are quite different from those for SMFRs. For the Lepping list events, there are a few mild peaks in the distribution of the azimuthal angle difference, for example, at $\Delta\phi \sim 0°$ and $\sim -140°$ (panel (e)), but those peaks are not pronounced. The Nishimura et al. list events also show a distribution with no pronounced peaks. Therefore, we suggest that the trend of the largely tilted, most often nearly perpendicular, orientation of flux ropes relative to the background IMF directions is a distinctive feature for SMFRs and not present for MCs.

Furthermore, we examined whether the statistical trend of SMFR orientations shown above is preferred by either type of helicity (chirality). For this purpose, we used only the SMFR events for which the azimuthal angle difference from the corresponding IMF directions is "sufficiently" close to 90°. Specifically, we selected 187 events out of the 261 SMFRs; these events satisfy $|\Delta\phi| = 90\overset{\circ}{.}9 \pm 35\overset{\circ}{.}2$ ($<1\sigma$). For these SMFRs, the percentage rate of each helicity, left-handed and right-handed, is 51% and 49%, respectively. The two upper panels of Figure 6 show the number of events in the parameter space of the azimuthal angle difference between the SMFR axis and the corresponding IMF directions, $\Delta\phi$, versus the corresponding IMF directions, $\langle \mathrm{IMF}\phi \rangle$. The presented results now distinguish between right- and left-handed helicity. The distribution in $\Delta\phi$ is concentrated at four locations for each helicity group. For the majority of the events, $|\Delta\phi|$ is somewhat more or less than 90°, approximately consistent with the trend in Figures 5(a)–(c). This is roughly equally true for both helicities of SMFRs and clear enough even though the number of events in each group is small (approximately 20). That is, the trend shown in Figures 5(a)–(c) remains valid even if helicities are distinguished.

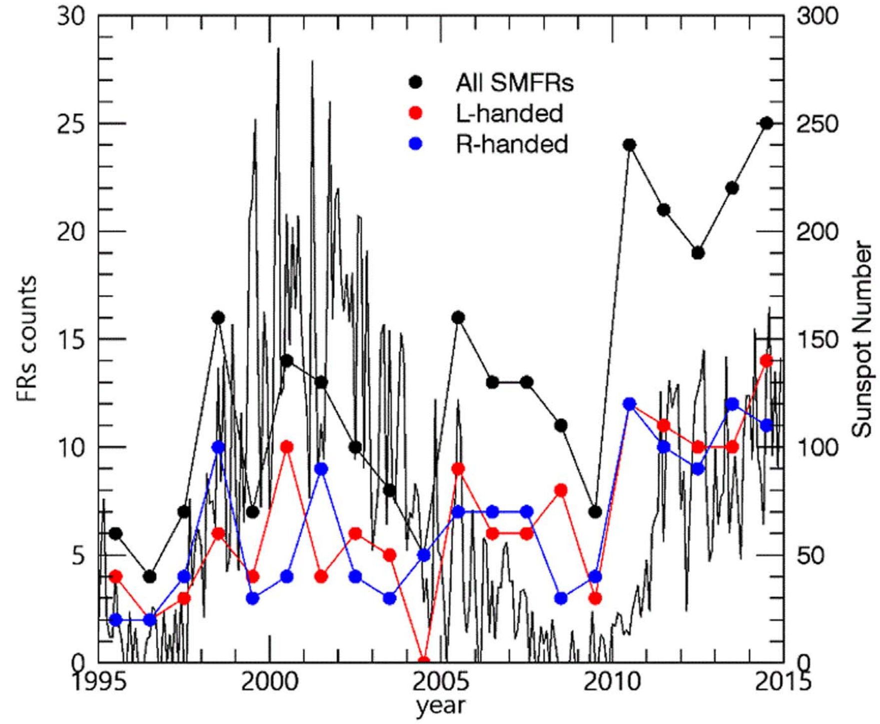

Figure 2. Yearly distribution of 261 SMFRs examined in this paper and the sunspot number distribution. The SMFR distribution is also distinguished by two helicities.

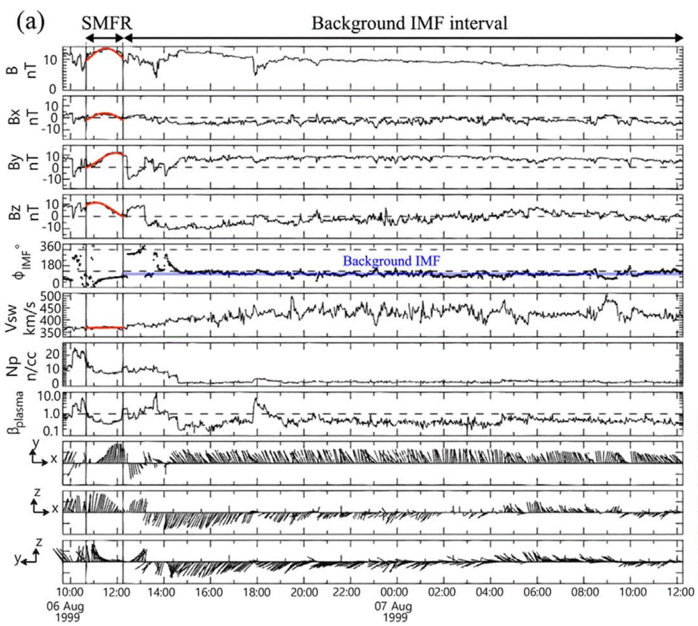

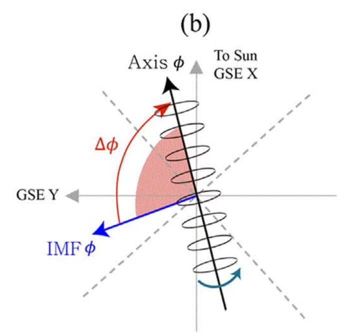

(c)

Start time	1999/08/06 10:40	Helicity	R
End time	1999/08/06 12:15	B_0 (nT)	18.2
Axis θ (°)	13.5	U_{sw} (km/s)	368
Axis ϕ (°)	13.8	R_0 (AU)	0.0033
IMF ϕ (°)	112.0	IP	-0.68
$\Delta\phi$ (°)	-98.2	E_{rms}	0.15

Figure 3. An example of an SMFR with force-free fitting results (the same event as in Figure 1(a)) and the corresponding background IMF conditions. (a) Solar wind parameters and interplanetary magnetic field observed by Wind. The two vertical lines denote the boundaries of the SMFR. The fitting curves are shown as red lines, and the bottom three panels show the magnetic vector evolutions. The background IMF interval is defined as one day after the end time of the SMFR. (b) Schematic for orientations of the SMFR (black arrow) and background IMF (blue arrow) on the *x*-*y* plane in the GSE coordinates. (c) Parameters obtained from the model fitting, including axis orientation (*Axis* θ and *Axis* ϕ), azimuthal angle of the background IMF (IMFϕ), relative difference between the azimuthal angles of the background IMF and SMFR axis ($\Delta\phi$), helicity (chirality) with R meaning right-handed helicity, axis magnetic field magnitude (B_0), flow speed (U_{sw}), flux rope radius (R_0), impact parameter (IP), and root-mean-squared error (E_{rms}).

Figures 6(c) and (d) show a schematic for eight categories of the event distributions in Figures 6(a) and (b) to further demonstrate the relationship among three parameters (azimuthal angle difference $\Delta\phi$, polarity of background IMF, and helicity). We should point out that the observed IMF polarity depends on the satellite location relative to the HCS, if the observations are made near the HCS. Depending on the satellite's location, an observed flux rope with a specific helicity can be found within either polarity of the background IMF. In this sense, the eight categories in Figures 6(a) and (b) can be reduced to four categories, i.e., A&D, B&C, E&H, and

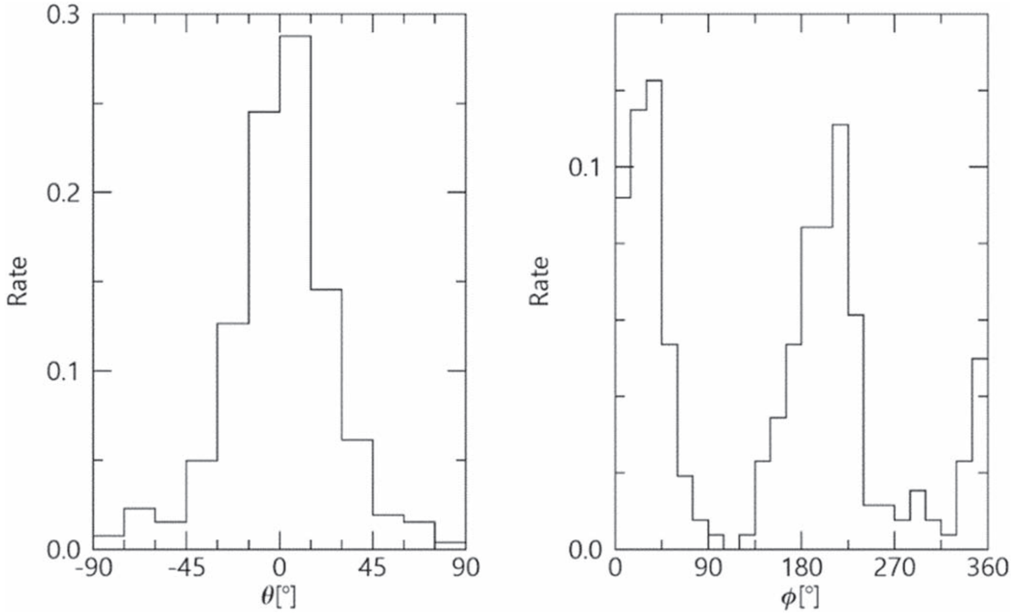

Figure 4. Statistics of the elevation (left) and azimuthal (right) angles of 261 SMFRs.

F&G, for flux ropes that are created at the HCS (see discussion in Section 4).

4. Discussion and Conclusion

In this work, we compared the azimuthal orientation of the SMFR axis with the direction of the background IMF and found that the axes of the majority of SMFRs tend to make large angles relative (and most often nearly perpendicular) to the background IMF. We emphasize that this finding is new and in contrast to previously reported results (Borovsky 2008; Hu et al. 2018; Chen & Hu 2020; Chen et al. 2021). The axial orientation for SMFRs identified at 1 au by the Grad–Shafranov reconstruction technique (Hu et al. 2018) was found to be mostly aligned along the Parker spiral. The results based on the same Grad–Shafranov reconstruction in Chen & Hu (2020) show that the azimuthal angles of the SMFRs identified at ∼0.3 to 1 au by Helios 1 and 2 and those at ∼6 to 8 au by Voyager 1 and 2 are broadly distributed without a pronounced peak. Most recently, Chen et al. (2021) identified SMFRs much closer to the Sun, using Parker Solar Probe observations, and their axial orientation distribution appears rather broad, with a mild peak at ∼120°–160° relative to the radial direction. On the other hand, Borovsky (2008) examined the flux tubes of the solar wind characterized by strong changes in the magnetic field direction from one tube to its neighbor. The axial directions of such flux tubes were obtained from the mean vector magnetic field within each flux tube, and they tended to be aligned with the Parker spiral but with significant spread. It is unclear to us at this time exactly what causes the discrepancy between these previous works and ours. However, we note that, in all these previous works, no direct, event-by-event comparisons were rigorously made with the actual corresponding background IMF directions. Additionally, we do not preclude the possibility that the events considered in those previous works as identified by different methods may be intrinsically (by origin or other unidentified features) different from ours.

The main finding in this work is also in stark contrast to the case of MCs. First, the axis azimuthal orientation of the MCs examined in our work does not indicate any strong preferred direction, as shown in Figure 5. Incidentally, we notice that a broad range of flux rope axis orientations (both in latitude and longitude) have been reported for MCs (e.g., Zhao & Hoeksema 1998). The orientation of MCs can be an interplanetary extension of that of the solar magnetic field surrounding a disappearing filament (e.g., Marubashi 1997; Zhao & Hoeksema 1998), whereas such an association is not yet clear for SMFRs. Second, there are reports (e.g., Rust 1994) suggesting that the helicity of MCs is consistent with that of solar filaments, which is in turn segregated by hemisphere. Such a relation is not known for SMFRs at the present time; the SMFRs selected here are evenly distributed between two helicities, and the main trend of the near-orthogonal azimuthal angle of the SMFR axis relative to the IMF is not biased by the choice of either helicity (shown in Figure 6).

A possible origin of SMFRs is the ejection of small flux ropes at the helmet streamer through magnetic reconnection. Recent Parker Solar Probe observations (Lavraud et al. 2020) indicate evidence of sequential reconnection at the helmet streamer tip causing a series of (either open or closed field) flux ropes embedded between successive high-density blobs (Sanchez-Diaz et al. 2017, 2019). The surrounding dense blobs may play a role in preventing an SMFR from expanding while propagating (Rouillard et al. 2009). In this illustration, it is possible to envision that the flux rope orientation at its birthplace makes a large angle (perhaps even 90°) relative to the background global field directions. Indeed, recent magnetohydrodynamic (MHD) simulations performed for $r = 1\ R_s$–$30\ R_s$ (Higginson & Lynch 2018) indicate the possibility that a small flux rope pinches off from the helmet streamer top and that the core field of the flux rope is oriented perpendicular to the radial direction. Also, Réville et al. (2020) exploit a 2.5D MHD model to show that the magnetic islands produced by reconnection near the tip of helmet streamers (through a tearing mode instability) are separated by additional smaller magnetic islands that may be more relevant to the SMFRs we identify in situ in this paper. These smaller simulated flux ropes are embedded in higher-density plasma (probably the bright blobs

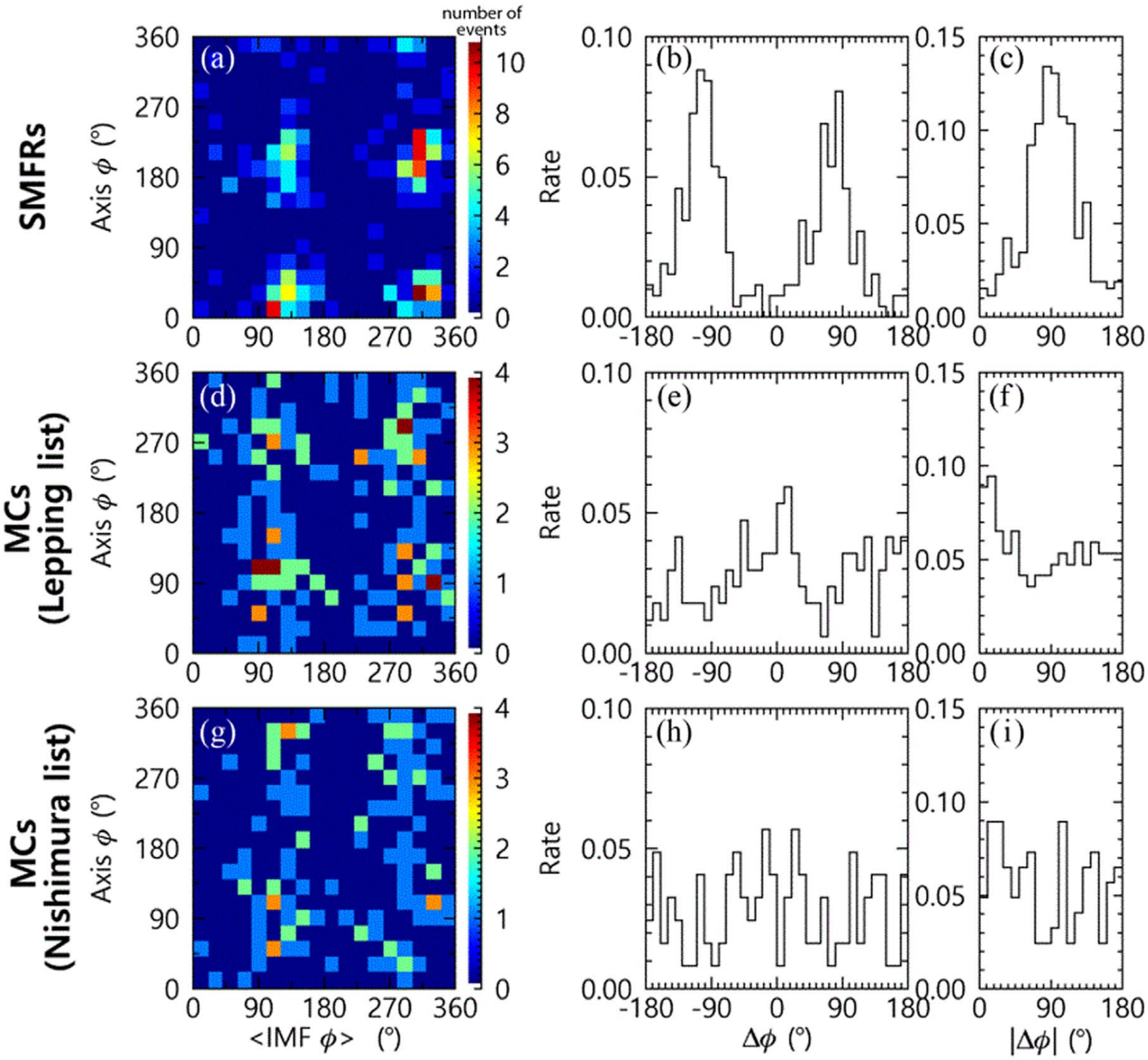

Figure 5. Statistics of azimuthal angles for SMFRs ((a)–(c)) and MCs ((d)–(i)) in comparison with those of the background IMF. The left column shows a color-coded number of events in the parameter space of the azimuthal angle of the flux rope axis vs. that of the corresponding background IMF. The center and right columns show the event rates as a function of azimuthal angle difference between the flux rope axis and corresponding background IMF ($\Delta\phi$ = SMFR *Axis* ϕ-*IMF*ϕ).

seen in white-light images) that separate the larger flux ropes. This has also been observed in 3D simulations by Réville et al. (2022). Most of the SMFRs we have studied in the present paper are also surrounded by elevated densities as shown in Figure 3. Observationally, it is unknown what the statistical distribution of the axial orientations of SMFRs would be if the majority of them were indeed created at helmet streamers. On the other hand, it has been suggested (Yurchyshyn 2008; Kay et al. 2015; Szabo et al. 2020) that significant evolution of solar ejecta (for example, a tendency to align with the HCS) occurs during propagation through interplanetary space, possibly changing their axial orientations (say, at 1 au) from those at generation points near the Sun. However, although many SMFRs are found near the HCS, some are not (Choi et al. 2021). Therefore, if most SMFRs were indeed launched near the Sun, a possible propagation effect implies that some other mechanism in interplanetary space, whether close to the HCS or not, must play a significant role in the robust statistical trend of the axial orientations found at 1 au in the present paper.

Another possibility is that multiple magnetic reconnections of previously open fields at the HCS in interplanetary space (well beyond the solar corona) can produce a flux rope (Moldwin et al. 1995). In this case, we can imagine that the flux rope axis makes a significant azimuthal angle to the background IMF direction, consistent with the main finding in the present work. On the other hand, Choi et al. (2021) have shown that the majority of low-β SMFRs at 1 au (practically the same event group as examined in the present paper) are connected to the Sun at one end (thus open field lines), and there is a very small fraction of SMFRs with closed field lines. Therefore, it needs to be verified whether flux ropes generated by interplanetary HCS reconnection meet this observational constraint for magnetic connectivity to the Sun. The same constraint also applies to flux ropes generated by turbulence in the solar wind (Greco et al. 2009; Telloni et al. 2016: Zheng and Hu et al. 2018; Pecora et al. 2019).

Future efforts should examine the possible connection of the orientation of the SMFR axis at 1 au and close to the Sun (using the recent Parker Solar Probe observations) to the neutral lines on the solar source surface, which can be done by using the potential field source surface (PFSS) map. This will help to

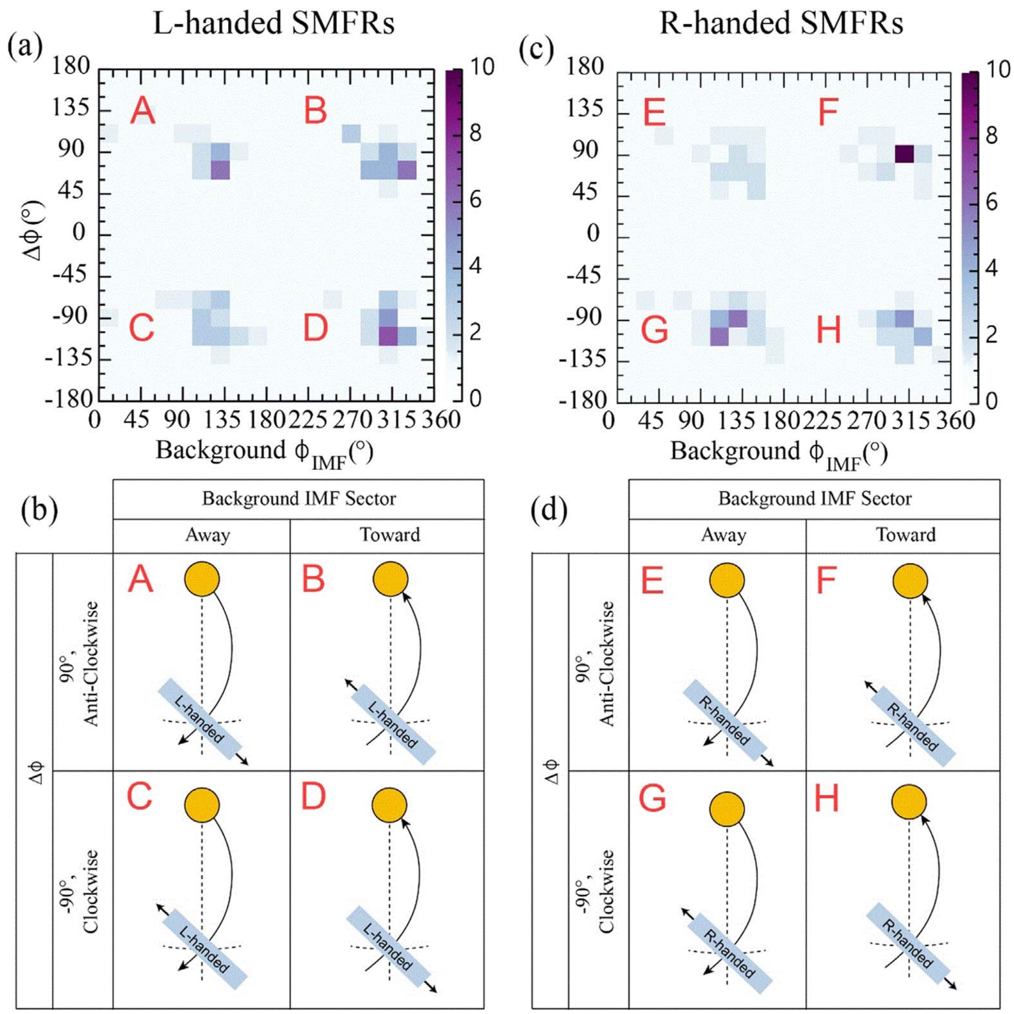

Figure 6. (a) and (c) Statistics of the azimuthal angle difference between SMFRs and background IMF vs. the background IMF azimuthal angle considering the helicity. (b) and (d) Schematic showing eight possible situations corresponding to the event groups in the upper panels.

determine whether an SMFR is formed by reconnection around the magnetic neutral sheet near the Sun.

In summary, we found a strong statistical trend in which the azimuthal direction of the SMFR axis makes a large angle, most often perpendicular to that of the background IMF direction. This is true independent of the magnetic helicity of SMFRs. This result is in stark contrast to previous reports for SMFRs and the cases of MCs, which do not exhibit such a trend. We suggest that this imposes an important constraint on scenarios regarding the origins and propagation physics of SMFRs whether they are due to solar origin or interplanetary origin.

The work by K.-E. Choi was supported by funding from the National Research Foundation of Korea grant 2021R1A6A3A01086361. D.-Y. Lee at Chungbuk National University acknowledges support from the National Research Foundation of Korea under grant NRF-2019R1A2C1003140. The WIND data used for this study are available at the cadweb.gsfc.nasa.gov site.

ORCID iDs

Kyung-Eun Choi https://orcid.org/0000-0003-2054-6011
Dae-Young Lee https://orcid.org/0000-0001-9994-7277

References

Borovsky, J. E. 2008, JGRA, 113, A08110
Cartwright, M. L., & Moldwin, M. B. 2008, JGRA, 113, A09105
Cartwright, M. L., & Moldwin, M. B. 2010, JGRA, 115, A08102
Chen, Y., & Hu, Q. 2020, ApJ, 894, 25
Chen, Y., Hu, Q., Zhao, L., et al. 2020, ApJ, 903, 76
Chen, Y., Hu, Q., Zhao, L., et al. 2021, ApJ, 914, 108
Choi, K.-E., Lee, D.-Y., Wang, H.-E., et al. 2021, SoPh, 296, 148
Drake, J. F., Agapitov, O., Swisdak, M., et al. 2020, A&A, 650, A2
Feng, H. Q., Chao, J. K., Lyu, L. H., et al. 2010, JGRA, 115, A09108
Feng, H. Q., Wu, D. J., Lin, C. C., et al. 2008, JGRA, 113, A12105
Greco, A., Matthaeus, W. H., Servidio, S., et al. 2009, ApJL, 691, L111
Higginson, A. K., & Lynch, B. J. 2018, ApJ, 859, 6
Hu, Q., Zheng, J., Chen, Y., et al. 2018, ApJS, 239, 12
Kay, C., Opher, M., & Evans, R. M. 2015, ApJ, 805, 168
Kim, M. J., Park, K. S., Lee, D.-Y., et al. 2017, JASS, 34, 237
Lavraud, B., Fargette, N., Réville, V., et al. 2020, ApJL, 894, L19
Lepping, R. P., Jones, J. A., & Burlaga, L. F. 1990, JGR, 95, 11957
Lepping, R. P., Wu, C.-C., Berdichevsky, D. B., et al. 2011, SoPh, 274, 345
Marubashi, K. 1997, in Geophysical Monograph 99, Coronal Mass Ejections, ed. N. U. Crooker, J. A. Joselyn, & J. Feynman (Washington, DC: AGU), 147
Marubashi, K., & Lepping, R. P. 2007, AnGeo, 25, 2453
Moldwin, M. B., Ford, S., Lepping, R., et al. 2000, GeoRL, 27, 57
Moldwin, M. B., Phillips, J. L., Gosling, J. T., et al. 1995, JGRA, 100, 19903
Nishimura, N., Marubashi, K., & Tokumaru, M. 2019, SoPh, 294, 49
Park, K. S., Lee, D.-Y., Kim, M. J., et al. 2018, JGRA, 123, 6307
Pecora, F., Greco, A., Hu, Q., et al. 2019, ApJL, 881, L11
Réville, V., Fargette, N., Rouillard, A. P., et al. 2022, A&A, 659, A110

Réville, V., Velli, M., Rouillard, A. P., et al. 2020, ApJL, 895, L20
Rouillard, A. P., Savani, N. P., Davies, J. A., et al. 2009, SoPh, 256, 307
Rouillard, A. P., Sheeley, N. R., Jr., Cooper, T. J., et al. 2011, ApJ, 734, 7
Rust, D. M. 1994, GeoRL, 21, 241
Sanchez-Diaz, E., Rouillard, A. P., Davies, J. A., et al. 2017, ApJ, 851, 32
Sanchez-Diaz, E., Rouillard, A. P., Lavraud, B., et al. 2019, ApJ, 882, 51
Shimazu, H., & Vandas, H. 2002, EP&S, 54, 783
Szabo, A., Larson, D., Whittlesey, P., et al. 2020, ApJS, 246, 47
Telloni, D., Carbone, V., Perri, S., et al. 2016, ApJ, 826, 205
Yu, W., Farrugia, C. J., Lugaz, N., et al. 2016, SoPh, 293, 165
Yurchyshyn, V. 2008, ApJL, 675, L49
Zhao, L.-L., Zank, G. P., Adhikari, L., et al. 2020a, ApJS, 246, 26
Zhao, L.-L., Zank, G. P., Hu, Q., et al. 2020b, A&A, 650, A12
Zhao, X. P., & Hoeksema, J. T. 1998, JGRA, 103, 2077
Zheng, J., & Hu, Q. 2018, ApJL, 852, L23
Zheng, J., Hu, Q., Chen, Y., et al. 2017, JPhCS, 900, 012024